Shortening the Reaction Pathway of Sulfur Redox Kinetics with 2,5-Dichloro-1,4-Benzoquinone to Minimize the Shuttle Effect in Lithium−Sulfur Batteries

Jiayi Shao, Hanxiao Wang, Xinjie Huang, Xianguo Ma, Xuyun Wang, Hongsheng Huang, Jianwei Ren,* and Rongfang Wang*

ABSTRACT: The low active material utilization, sluggish sulfur redox kinetics, and formation of unstable interfacial layers remain critical challenges in lithium−sulfur (Li−S) batteries. To minimize these effects, 2, 5-dichloro-1,4-benzoquinone (DCBQ) was demonstrated in this study as an electrolyte additive. Leveraging its unique symmetrical structure, DCBQ interacted with polysulfides during charge and discharge cycles to form insoluble symmetric cyclic organic polysulfide intermediates. These intermediates served as a cathode-electrolyte interphase (CEI) by attaching to the sulfur cathode surface, which mitigated the shuttle effect by reducing the accumulation of insoluble Li_2S and suppressing polysulfide dissolution. In the presence of DCBQ, the discharge pathway for Li_2S_6 transitioned from $Li_2S_6 \rightarrow Li_2S_4 \rightarrow Li_2S_2 \rightarrow Li_2S$ to a shortened sequence of $Li_2S_6 \rightarrow Li_2S_3 \rightarrow Li_2S$, enhancing sulfur utilization and streamlining redox processes. On the anode side, the formation of LiCl and intermediate compounds contributed to an organic−inorganic solid-electrolyte interface (SEI), which protected the lithium anode, improved the Li^+ diffusion coefficient (6.63×10^{-11} cm^2 S^{-1}), and eventually enhanced the battery's cycling stability. Consequently, the Li−S battery that included the DCBQ additive exhibited nearly 100% Coulombic efficiency at a rate of 0.2 C. It showed an initial discharge-specific capacity of 992.24 mAh g^{-1} and experienced a low-capacity degradation of just 0.45% per cycle over 120 cycles. These results highlight the effectiveness of DCBQ as an electrolyte additive in enhancing both the performance and stability of the battery.

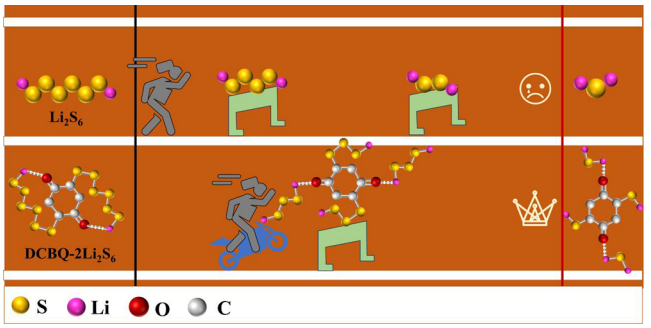

KEYWORDS: *insoluble symmetric cyclic organic polysulfide intermediates, shortened redox pathway, cathode-electrolyte interphase (CEI), shuttle effect, lithium−sulfur batteries*

1. INTRODUCTION

Recent advancements in mobile electronics and new energy vehicles have positioned lithium−sulfur (Li−S) batteries, with a theoretical specific capacity of 2600 Wh kg^{-1}, as a promising energy storage solution. Compared to conventional lithium-ion batteries, Li−S batteries offer distinct advantages, including high energy density, cost-effective and abundant raw materials, and environmental sustainability.[1−3] However, their widespread adoption faces challenges rooted in the inherent properties of electrode materials. Both S_8 and the end discharge product (Li_2S) are insulating materials for the sulfur (S) cathode.[4−6] Additionally, during discharge, the dissolution of lithium polysulfides (Li_2S_n) into the electrolyte initiates the phenomenon known as the "shuttle effect".[7,8] Additionally, the significant volume expansion (~80%) experienced during the reaction reduces the utilization efficiency of active materials while accelerating the decay of discharge-specific capacity.[9−11] Scheme 1a depicts the widely accepted reaction mechanism for the sulfur cathode. During discharge, S_8 reacts with Li^+ to produce soluble long-chain lithium polysulfides (Li_2S_n, $4 \leq n \leq 8$), contributing approximately 25% of the theoretical capacity. As the discharge progresses, these long-chain polysulfides are converted into short-chain species (Li_2S_n, $2 \leq n < 4$) before forming insoluble Li_2S. This final conversion accounts for around 75% of the theoretical capacity but represents the slowest and most kinetically limiting step of the reaction.

To respond to the "shuttle effect" resulted from the slow redox kinetics and dissolution of polysulfides, researchers have implemented a series of improvement strategies. One of the most common approaches is immobilizing polysulfides to reduce their shuttling. Carbon porous materials have been

Scheme 1. Schematic Effects of Different Additives on Sulfur Redox Pathways[a]

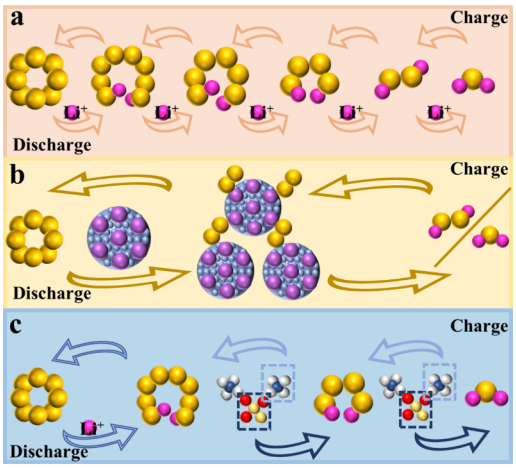

[a](a) Conventional sulfur redox pathway: $S_8 \rightleftharpoons Li_2S_8 \rightleftharpoons Li_2S_6 \rightleftharpoons Li_2S_4 \rightleftharpoons Li_2S_2 \rightleftharpoons Li_2S$; (b) TiONQDs@C as a redox mediator to shorten the pathway: $S_8 \rightleftharpoons S_2^{\sigma-}\text{-}RM^{\sigma+} \rightleftharpoons Li_2S_2/Li_2S$;[27] (c) AMTS additive shortening the redox pathway: $S_8 \rightleftharpoons Li_2S_8 \rightleftharpoons Li_2S_4 \rightleftharpoons Li_2S$.[28]

extensively explored as sulfur-anchoring materials.[12] However, the limited specific surface area of solid materials restricts their ability to immobilize polysulfides. To strengthen the interaction between polysulfides and the cathode, polar materials such as elemental metals,[11,13,14] metal oxides/nitrides/sulfides,[15−21] as well as metal−organic frameworks (MOFs)[22−24] have been explored extensively on the active sites to immobilize Li_2S_n, catalyze its conversion and promote redox kinetics. However, the expansion of the sulfur cathode during cycling can lead to irreversible structural collapse of the added porous carbon materials, which significantly shortens the lifespan of the active cathode materials.[25,26] Additionally, providing a protective layer for the sulfur cathode has also been widely adopted. For instance, N-bromosuccinimide (NBP) was employed by Wu et al.[8] as an electrolyte additive in Li−S batteries. This additive promoted the in situ formation of an organic polysulfide deposition layer, which effectively prevented the dissolution and diffusion of polysulfides. Consequently, the NBP-incorporated Li−S battery kept a discharge-specific capacity of 700 mAh g^{-1} after 50 cycles at 0.1 C. Moreover, altering the reaction pathway of polysulfides offers a promising approach, yet relatively underexplored. For example, Li and Ma et al.[27] introduced TiO_xN_y-TiO_2 quantum dots embedded in carbon composites (TiONQDs@C) as a redox mediator (RM). This mediator facilitated the direct conversion of S_8 to $S_2\sigma$--RMσ+, followed by the sequential formation of Li_2S_2 and Li_2S during discharge (Scheme 1b). By circumventing the formation of soluble polysulfides, this approach achieved an exceptionally low-capacity decay rate of just 0.02% per cycle. However, the one-step annealing method lacks the precision required to control the structure of carbon materials, highlighting the need for more advanced and effective strategies to stabilize sulfur species. Liu et al.[28] employed ammonium thiosulfate (AMTS) as an effective electrolyte additive in promoting the redox reaction of polysulfides. Their approach facilitated the swift transformation of long-chain polysulfides into short-chain counterparts, and thereby reduced polysulfide accumulation (Scheme 1c). However, these reactive additives pose a risk of corrosion to the Li anode. This highlights the necessity for a strategy that can simultaneously immobilize polysulfides and enhance their conversion without compromising the stability of the lithium anode.

In this study, 2,5-dichloro-1,4-benzoquinone (DCBQ) was introduced as an additive in electrolyte to promote the redox kinetics of Li_2S_n and establish an organic interfacial protection layer on the sulfur cathode, enhancing the utilization of active materials. The symmetric carbonyl oxygen and halogen

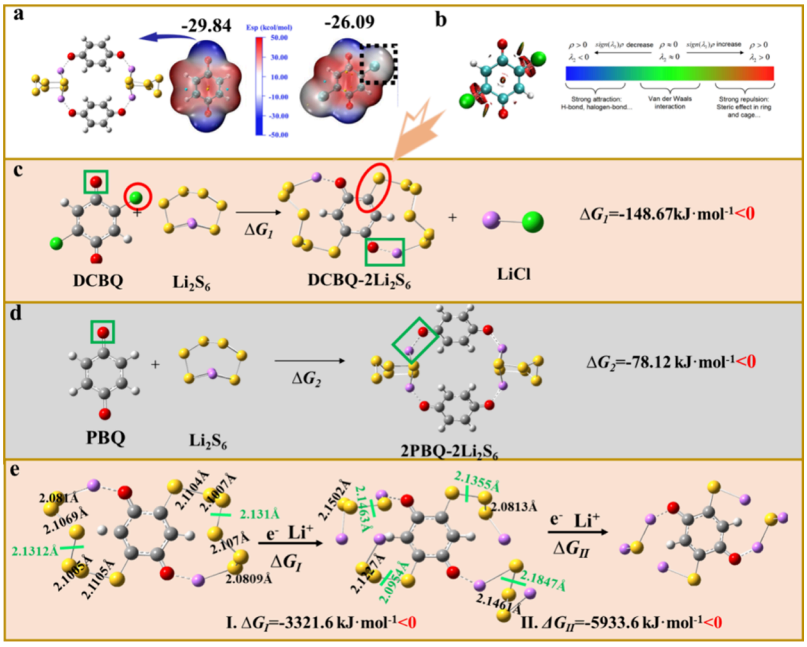

Figure 1. (a) Electrostatic potential (ESP) maps for the PBQ and DCBQ molecules. (b) Weak interactions within the DCBQ molecule, as revealed by RDG analysis. (c) Gibbs free energy DCBQ in reacting with Li_2S_6. (d) Gibbs free energy of PBQ in reacting with Li_2S_6. (e) Schematic representation of the bond-breaking process of cyclic organic sulfur intermediate during discharge, with Gibbs free energy for each reaction step.

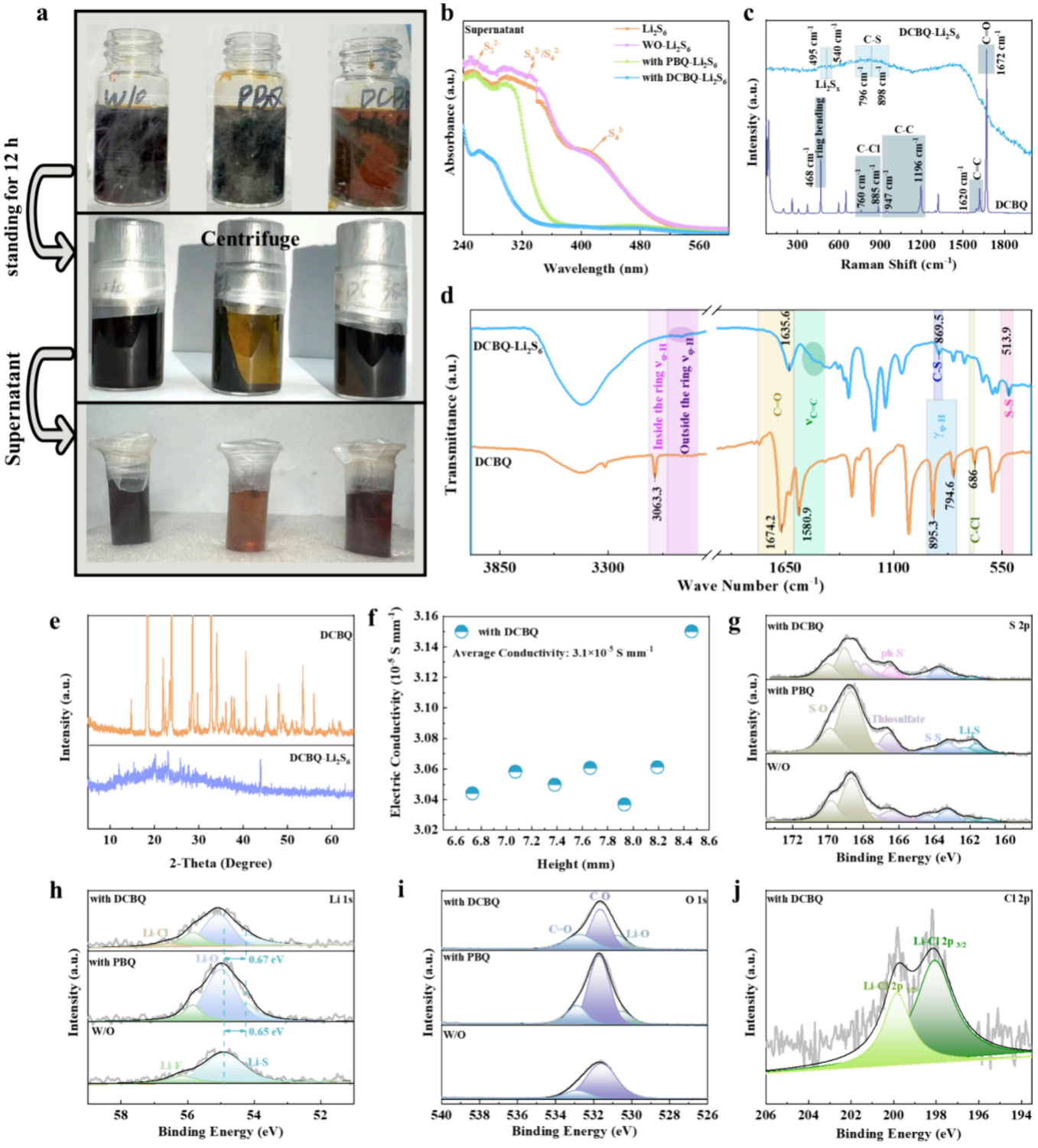

Figure 2. (a) Visualization of the adsorption of Li_2S_6 by electrolyte additives and blank electrolyte, (b) UV spectra of the supernatant after three samples absorbed Li_2S_6, (c) Raman spectra, (d) infrared spectra, and (e) XRD patterns of DCBQ and DCBQ-Li_2S_6, (f) the electric conductivity of the DCBQ-Li_2S_6 intermediate. High-resolution XPS spectra of three samples at (g) S 2p, (h) Li 1s, (i) O 1s, and (j) Cl 2p.

functional groups in DCBQ interacted with Li_2S_n during discharge via Li−O and C−S bonds, resulting in the formation of an insoluble, conductive cyclic organic sulfur intermediate. This intermediate not only enabled efficient electron transfer within sulfur species but also confined them to the cathode side. By facilitating the conversion of long-chain polysulfides into shorter chains, DCBQ notably enhanced the redox kinetics of Li_2S_n.

2. EXPERIMENTAL SECTION

2.1. Synthesis of Fe-NC Sample. To synthesize the Fe-NC sample, 0.03 mmol of $Fe(NO_3)_3$ and 1 g of peptone were dissolved in 10 mL of deionized water. The resulting solution was placed in a refrigerator and allowed to freeze for 12 h. Following freeze-drying,

the sample was mixed with 10 g of NaCl, and the mixture underwent ball milling for 3 h. The ball-milled sample was subsequently heated to 900 °C at a heating rate of 5 °C min^{-1} in N_2 atmosphere. The sample was kept at this temperature for 1 h. After cooling, the sample was thoroughly washed with deionized water and dried for subsequent use.

2.2. Synthesis of S@Fe-NC Sample. The Fe-NC sample was mixed with sublimed sulfur in a 3:7 mass ratio and ground for 30 min. The resulting mixture was then moved to an argon-filled glovebox and heat-treated in an oven at 155 °C for 12 h. The final product obtained is S@Fe-NC.

2.3. Synthesis of Li_2S_6 Solution. Li_2S and sublimed sulfur were combined in a molar ratio of 1:5 and introduced into a solution containing 1,3-dioxolane (DOL) and dimethoxyethane (DME) in equal volume proportions. The mixture was stirred at 60 °C for 24 h, resulting in a 0.2 M Li_2S_6 solution. Similarly, a 5 mM Li_2S_6 solution was prepared using the same method.

2.4. Preparation of Electrolyte Additives. A blank electrolyte was formulated by dissolving 1.0 M lithium bis-(trifluoromethanesulfonyl)imide (LiTFSI) and 0.1 M $LiNO_3$ in a 1:1 volume mixture of 1,3-dioxolane (DOL) and dimethoxyethane (DME). P-benzoquinone (PBQ) and 2,5-dichloro-1,4-benzoquinone (DCBQ) were then incorporated into the electrolyte at concentrations of 60, 70, and 80 mM, respectively. According to the testing results presented in Figure S1, 70 mM concentration was identified as optimal, and this concentration was used for all subsequent experiments.

3. RESULTS AND DISCUSSIONS

To predict the binding interactions between polysulfides and electrolyte additives, the weak intermolecular interactions[29−31] and electrostatic potential (ESP) of PBQ and DCBQ were calculated.[32−34] The ESP results in Figure 1a suggest that the electrostatic potential near the carbonyl oxygen is the most negative (−29.84 kJ mol^{-1}), making it a reactive site that forms a Li−O bond with polysulfides. This is because PBQ contains two electron-withdrawing carbonyl oxygen groups at the para positions, which attract electron density from the benzene ring, concentrate electrons around the carbonyl oxygen and increase its electrophilicity. In the case of DCBQ, two Cl substituents at the 2 and 6 positions further contribute to the electron-withdrawing effect. Cl attracts some electron density from the carbonyl oxygen, but the electronegativity of O is higher than that of Cl, so the electron cloud shifts toward the carbonyl oxygen. This raises the electrostatic potential of the carbonyl oxygen to −26.09 kJ mol^{-1}, facilitating the binding of polysulfides to the carbonyl oxygen through an ionic interaction, resulting in the formation of a Li−O bond. In addition, analysis of the intermolecular weak interactions (RDG) reveals that there is a steric hindrance effect between the carbonyl oxygen structure and the adjacent halogen-substituted group in the DCBQ molecule. As a result, when polysulfides react with DCBQ, they preferentially interact with the halogen-substituted group in the meta position (Figure 1b). It is well-known that polysulfides readily undergo nucleophilic substitution reactions with the halogen-substituted group, breaking the C−Cl bond to form a C−S bond. The resulting chlorine free radical will then combine with lithium to form LiCl. As illustrated in Figure 1c,d and Table S1, the reaction Gibbs free energy (ΔG) for binding the two additives and Li_2S_6 was calculated using Shermo.[35] The negative values of ΔG_1 (−148.67 kJ mol^{-1}) and ΔG_2 (−78.12 kJ mol^{-1}) indicate that these processes are thermodynamically spontaneous. This insoluble cyclic organic sulfur intermediate not only forms an electrochemical interface layer on the sulfur cathode, preventing the accumulation of insoluble Li_2S on its surface and ensuring the active material's participation in reactions, but also creates an organic−inorganic interface layer on the lithium anode, protecting it from polysulfide corrosion and preventing irregular dendrite growth. Theoretical studies of the reaction mechanism of insoluble intermediates during the discharge process were carried out through Gibbs free energy calculations. As shown in Figure 1e, the S−S bond length between the third and fourth positions of DCBQ-2Li_2S_6 is the longest (2.13 Å). This suggests that during discharge, lower bond dissociation energy is required to break the bond and form DCBQ-4Li_2S_3, which ultimately results in the formation of DCBQ-4Li_2S. This shortens the original long-chain reaction ($S_6^{2-} \leftrightarrow S_4^{2-} \leftrightarrow S_2^{2-} \leftrightarrow S^{2-}$), and thus promotes the conversion of polysulfides. Additionally, cyclic voltammetry (CV) tests reveal the presence of Li_2S_3 between 2.1 and 2.2 V.[35] Therefore, the battery with the DCBQ additive was tested at a scan rate of 0.05 mV s^{-1}, and a reduction peak around 2.13 V was observed, which can be attributed to the presence of Li_2S_3 (Figure S2). This further demonstrates that the addition of DCBQ can shorten the sulfur conversion process. In contrast, 2PBQ-2Li_2S_6 follows the original path during discharge and does not shorten the reaction pathway (Figure S3). Additionally, the redox properties of the intermediate are closely related to the frontier molecular orbital (FMO) energy levels, as shown in Figure S4.[36] Typically, the lower of the lowest unoccupied molecular orbital (LUMO) energy level, the easier it is for the molecule to accept electrons, increasing its oxidizing ability and making it more easily reduced. The incorporation of DCBQ notably decreases both of the LUMO energy level and energy gap. The energy gap reflects the ease of electron transition from the occupied to the unoccupied orbitals-smaller energy gaps mean the compound is more likely to undergo electron transitions and thus more readily participate in reactions.[33,37] The addition of DCBQ not only alters the reaction pathway of polysulfides but also further accelerates their redox rate, thereby improving sulfur utilization.

To demonstrate the formation of insoluble cyclic organic sulfur intermediates, a visualization experiment was conducted. As demonstrated in Figures 2a and S5a,b, 0.7 M of Li_2S_6 was added to two types of additives and blank electrolyte. Insoluble organic sulfur intermediate precipitates immediately appeared in the sample bottles with the added additives. After standing for 12 h, the sample bottle with DCBQ contained more precipitate, indicating that the addition of DCBQ promotes the reaction with Li_2S_6 and stabilizes it. After centrifuging the mixture, the supernatant in the DCBQ-added sample bottle changed from a cloudy red-black color to a clear purple, confirming that a reaction occurred between the two during the standing process. UV testing was then conducted on the supernatant. As shown in Figure 2b, the sample containing only Li_2S_6 shows peaks at 253, 298, and 412 nm. They are corresponding to S_2^{2-}, S_6^{2-}/ S_4^{2-} and S_4^{2-}, respectively.[28] The UV peaks in the supernatant with the additives were significantly weakened, and the peak at 412 nm even disappeared. This indicates that the additives bound Li_2S_6 in the precipitate. In contrast, the UV peaks of the blank electrolyte were nearly identical to those of pure Li_2S_6, suggesting that the blank electrolyte did not play a role in stabilizing Li_2S_6. To examine the chemical bonding structure of the insoluble intermediate, Raman spectroscopy was used. The Raman spectra of DCBQ and DCBQ-Li_2S_6 samples are

displayed in Figure 2c. The vibration peak at 441 cm^{-1} is associated with the bending vibration of the benzene ring,[38] whereas the peaks at 760 and 885 cm^{-1} correspond to the C−Cl bonds located at the para positions on the benzene ring. The stretching vibration peaks of most C−Cl bonds are observed between 700 and 800 cm^{-1},[39,40] which is due to the shift of the vibration peaks caused by functional group aggregation. The vibration peaks at 1620 and 1672 cm^{-1} account for the stretching vibrations of the C═C and two para-positioned C═O bonds on the benzene ring, respectively, and the peaks at 947 and 1196 cm^{-1} are from the expansion vibration of C−C bonds within the benzene ring.[41,42] In the Raman spectrum of DCBQ-Li_2S_6, the peaks corresponding to the original C−Cl bonds in the additive are no longer present. Instead, they are replaced by vibration peaks for C−S bonds at 796 and 898 cm^{-1}. Furthermore, peaks associated with lithium polysulfides are observed at 495 and 540 cm^{-1}, suggesting that the insoluble organic sulfur intermediate not only retains the original benzene ring structure but also forms new C−S bonds with the polysulfides. In contrast, the Raman spectrum of the PBQ-Li_2S_6 sample keeps the structure of quinone but only shows vibration peaks related to the polysulfides. This suggests that the intermediate serves solely to stabilize the polysulfides without reacting with them to form new bonds (Figure S5c), which is consistent with the computational results. To further confirm the above analysis, infrared spectroscopy was performed on the two insoluble intermediates. As shown in Figure 2d, the infrared spectrum of DCBQ shows vibration peaks at 3063.3 and 2928 cm^{-1}, and they are associated with the stretching vibrations of the aromatic hydrogen both inside and outside the ring. The peaks at 1674.2 and 1580.9 cm^{-1} belong to the stretching vibrations of C═O and C═C on the benzene ring, respectively. The two peaks at 895.3 and 794.6 cm^{-1} speak to the bending vibrations of the aromatic hydrogen, indicating the presence of a tetra-substituted structure, while the peak at 686 cm^{-1} corresponds to the C−Cl substitution.[43] In the infrared spectrum of the additive combined with Li_2S_6, it can be observed that the vibration peak originally assigned to C−Cl disappears, replaced by a C−S bond vibration at 869.5 cm^{-1}. Additionally, a peak for S−S bonds appears at 513.9 cm^{-1}.[44] These features are not observed in the infrared spectrum of PBQ-Li_2S_6 (Figure S5d), which aligns with the conclusions from the Raman analysis. XRD analysis of the insoluble intermediates in Figures 2e and S5e reveals some peaks from the additives in the precipitate, suggesting that the additives have spontaneously reacted with Li_2S_6 during the chemical reaction. This further confirms that the structure of this insoluble intermediate is consistent with the structure obtained from computational calculations. To verify whether the insoluble intermediate affects the electronic conductivity inside the working electrode, conductivity tests were performed. As shown in Figures 2f and S5f, the insoluble organic sulfur intermediate exhibits an electric conductivity of $\sigma_{DCBQ\text{-}Li_2S_6} = 3.1 \times 10^{-5}$ S mm^{-1}. This suggests that, during the discharge process, electrons are able to traverse the solid electrolyte interphase (SEI) layer, facilitating electron transfer within the working electrode and minimizing the buildup of insulating Li_2S in the electrode.

To analyze the composition of the cathode's CEI film in a Li−S battery, X-ray photoelectron spectroscopy (XPS) was performed on the sulfur cathode after 50 cycles at a rate of 0.2 C. Figure 2g shows the deconvoluted S 2p spectrum. Peaks appeared at 161.9 and 162.85 eV correspond to Li_2S,[45] while those at 163.75 and 164.75 eV are attributed to S−S bonds.[37] Polysulfide (thiosulfate) peaks appear at 167.9 and 168.45 eV, which arise from side reactions between lithium nitrate and polysulfides during discharge.[46−49] The shift in the peak position of thiosulfate after the addition of DCBQ additive is primarily due to the interaction between DCBQ and polysulfides, which alters their primary redox pathways. This interaction increases the bond energy of the lithium−oxygen and carbon−sulfur bonds, thereby enhancing the binding energy of the sulfur atoms, and ultimately causing the thiosulfate peak to shift to a higher binding energy position.[50,51] Second, the added DCBQ additive exhibits oxidizing properties,[52] which may elevate the oxidation state of the sulfur atoms in thiosulfate, leading to an increase in binding energy. Lastly, DCBQ reacts with polysulfides to form an insoluble organic sulfur intermediate, which adsorbs on the sulfur cathode surface, altering the chemical environment of thiosulfate and consequently affecting the binding energy. The appearance of S−O bonds at 169.05 and 170.05 eV suggests the decomposition of lithium salts. After incorporating the DCBQ additive, new peaks at 166.45 and 167.2 eV emerge, which correspond to the ph-S bonds formed between DCBQ and polysulfides.[53] This observation is further confirmed by the C 1s spectrum in Figure S5g. Additionally, the significantly reduced peak area for Li_2S indicates that the DCBQ additive effectively prevents the insulating Li_2S from accumulating on the working electrode surface. Further analysis of the Li 1s spectrum (Figure 2h) reveals the presence of Li−S and Li−F peaks at 54.25 and 55.85 eV,[54] respectively. The two new peaks at 55.1 and 56.6 eV correspond to Li−O[55,56] and Li−Cl[57] bonds, respectively. The presence of these peaks is also confirmed in the O 1s (Figure 2i) and Cl 2p (Figure 2j) spectra, reinforcing that during discharge, the additive reacts with polysulfides to form a new insoluble intermediate, consistent with the computational results. The additive also safeguards the Li anode from polysulfide corrosion by contributing to the formation of a SEI layer on the surface. To examine the composition of the organic−inorganic SEI layer, XPS analysis was carried out. Figure S6 presents the Cl 2p, Li 1s, O 1s, and S 2p spectra of the Li−S battery after cycling. The Li 1s XPS spectrum in Figure S6c displays peaks at 54.3 and 55.0 eV, which are associated with Li−S and Li−O bonds, respectively. Peaks of Li−F (55.5 eV) and Li−Cl (56.1 eV) bonds aligning with the Li−Cl peak in Figure S6d confirm the existence of the inorganic SEI layer. Additionally, when various additives were added, the peaks in the Li 1s spectrum shifted toward the lower binding energies. For the Li−S bond, the sample with DCBQ shows a shift of 0.65 eV, while the sample with PBQ shifts by 0.09 eV. In the O 1s spectrum (Figure S6b), the peak shifts toward higher binding energies. This shift occurs due to the electron transfer from the oxygen in the quinone-based additives to the lithium in the polysulfides during discharge. The more significant shift observed with DCBQ is due to the electron-withdrawing nature of the carbonyl oxygen and chlorine on the benzene ring, which increases electron density around them and enhances interaction with polysulfides.[53] From the S 2p spectrum in Figure S6a, peaks at 160.0 and 161.4 eV correspond to Li_2S_2/Li_2S, indicating that polysulfides have shuttled to the lithium anode and were reduced on its surface, causing anode corrosion. Peaks at 162.0 and 163.1 eV belong to sulfur-containing organic compounds, products of the

reaction between DCBQ and polysulfides, confirming the presence of the organic SEI layer.

Combining the experimental and theoretical findings, it can be concluded that the inclusion of the DCBQ additive fulfills two primary functions. First, it forms a conductive, insoluble intermediate with polysulfides that attaches to the sulfur cathode surface. This intermediate facilitates efficient electron transfer within the sulfur species and prevents the buildup of insulating Li_2S on the sulfur cathode surface, which would otherwise impede the involvement of active materials in the reaction (Figure 3a). Second, during discharge, polysulfides

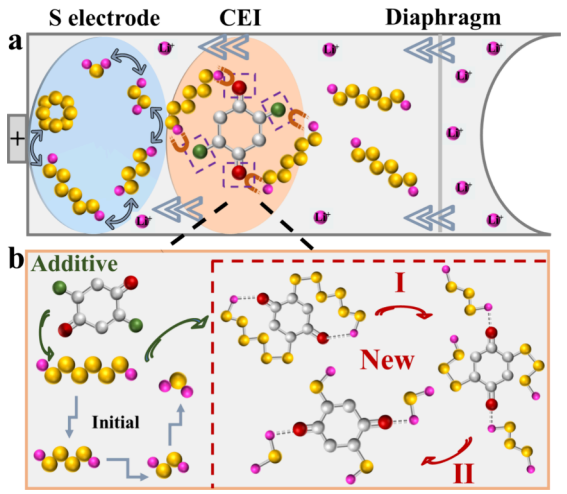

Figure 3. Schematic diagram of the interaction between DCBQ and Li_2S_x for (a) the sulfur cathode and (b) the sulfur redox pathway "DCBQ-2Li_2S_6↔DCBQ-4Li_2S_3↔ DCBQ-4Li_2S".

need to undergo a transformation from Li_2S_6 to Li_2S_4, then to Li_2S_2, and finally to Li_2S. The conversion from Li_2S_4 to Li_2S_2 involves a phase transition from liquid to solid, which is a slow process. However, after the addition of DCBQ, the organic sulfur intermediate formed by the reaction with Li_2S_6 can alter the original pathway, reducing the conversion binding energy and accelerating the conversion rate (Figure 3b). Specifically, DCBQ-2Li_2S_6 is converted to DCBQ-4Li_2S_3 during discharge, which then directly transforms into DCBQ-4Li_2S, providing a new pathway for the redox reactions of polysulfides.

To examine the effect of the insoluble symmetric cyclic organic sulfur intermediate, formed by the interaction of DCBQ with polysulfides, on the sulfur cathode interface structure, scanning electron microscopy (SEM) images of the working electrodes were taken after 50 cycles at 0.2 C. The analysis compared cells with and without the DCBQ additive. As illustrated in Figures 4a–f and S7a–c, the working electrode without the additive shows deeper cracks and a rougher surface, whereas the working electrode of the DCBQ-added sample (Figure 4d–f) has fewer cracks and a more compact surface. This suggests that during charge–discharge cycles, the insoluble cyclic organic sulfur intermediate reduces the adhesion of lithium polysulfides to the electrode, thereby minimizing the loss of active material. Figure 4g,h shows the side views of working electrodes for both samples. The sample with the blank electrolyte exhibits a rough, disordered surface (29 μm) and shows signs of electrode consumption, while the DCBQ-added sample shows a compact and flat CEI layer (10 μm). This observation suggests that the organic sulfur intermediate adheres to the sulfur cathode surface, promoting

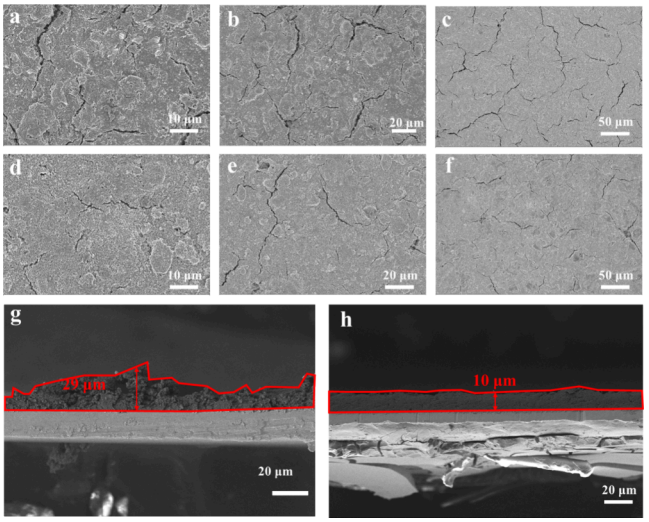

Figure 4. (a–c) The vertical view of the sulfur cathode after 50 cycles at 0.2 C in a Li–S battery using blank electrolyte as control, and (d–f) the sulfur cathode with DCBQ at different magnifications. (g) The side view of the sulfur cathode for the control battery, and (h) side view of the sulfur cathode with DCBQ.

efficient electron transfer within the sulfur and reducing the deposition of lithium polysulfides. Ultimately, this enhances the utilization of the active material by reducing its loss. To further probe the influence of electrolyte additives on the interface structure of lithium anode, the morphology of the lithium metal electrode was examined after 50 cycles at 1 mA cm^2 in a lithium–lithium symmetric cell using SEM. As observed in Figure S8a–c, the lithium metal surface of the sample with the blank electrolyte displays an irregular appearance with large cracks and a rough surface. The side view (Figure S8j) shows a SEI layer that is thick, uneven, and loosely structured. This formation results from the ongoing disruption and reformation of the interface layer as lithium metal reacts with lithium nitrate during the discharge. This results in an irregular SEI layer and causes volume expansion. In contrast, the battery with electrolyte additives (Figure S7d–i) shows a smooth lithium metal surface without obvious dendrites and a compact, flat SEI layer, with the DCBQ sample performing the best (Figure S8h–i). This is because DCBQ reacts with a small amount of polysulfides that have migrated to the lithium anode, forming an insoluble symmetric cyclic organic sulfur intermediate. This intermediate attaches to the lithium metal surface, forming an organic SEI layer (Figure S8l) that isolates polysulfides. Additionally, sulfur from the polysulfides substitutes chlorine to form the LiCl inorganic SEI layer, achieving organic–inorganic SEI coprotection of the lithium anode. To verify the primary components of the interface protective layer, batteries containing the additives and blank control batteries were cycled for 80 cycles at 0.2 C. Afterward, the lithium foil was removed, and the side interface protective layer was subjected to EDS analysis, as shown in Figure S9a–c. In the SEI layer of the lithium anode in the blank control battery, only Li and S elements were present. In the SEI layer of the anode with PBQ additive, elements O and C were also detected. This indicates that the primary components of the interface layer are organic insoluble intermediates. In the SEI layer of the anode with DCBQ additive, Cl elements were additionally detected, which suggests that the interface protective layer consists of both

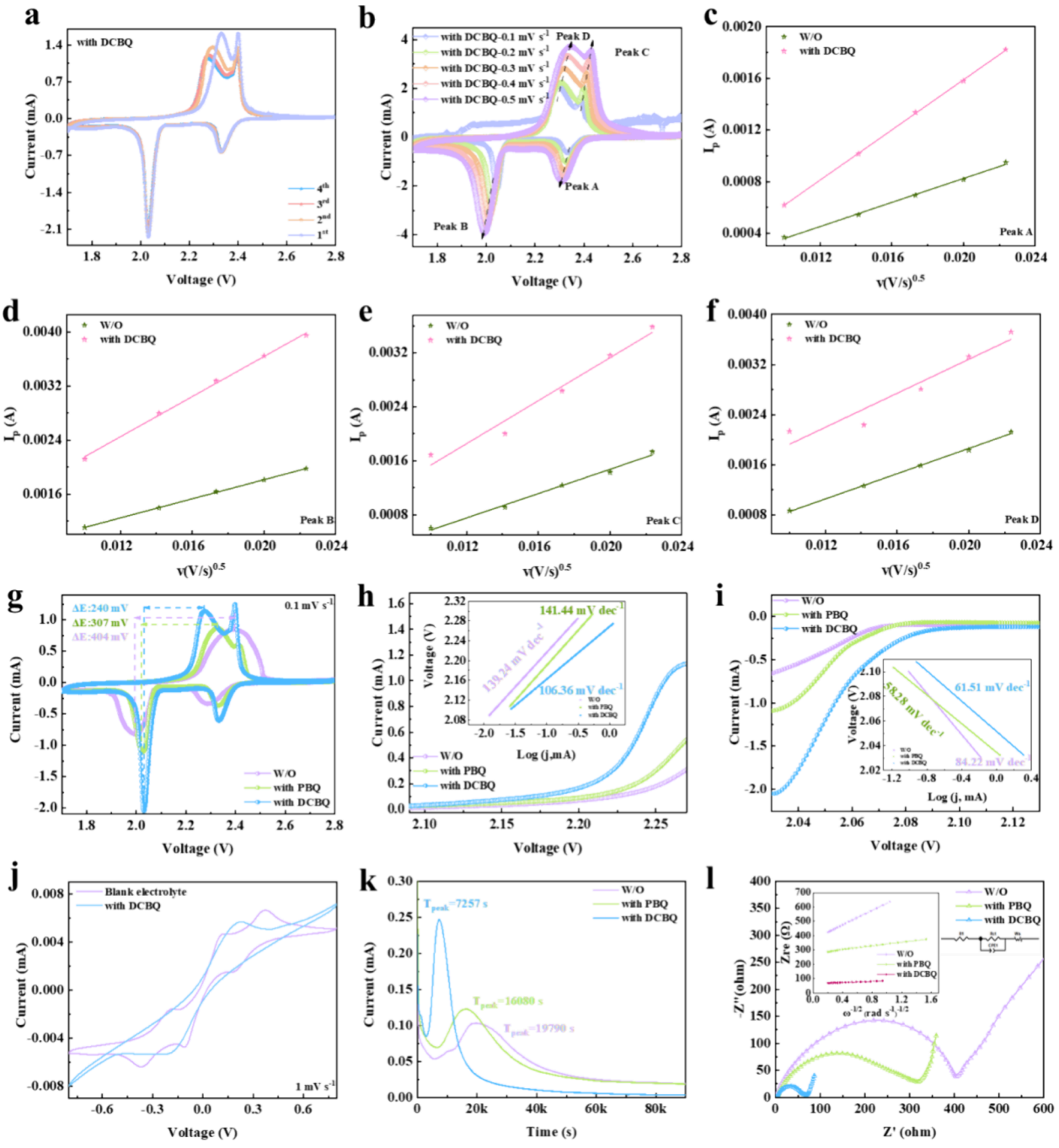

Figure 5. (a) Initial CV curve of DCBQ at a scan rate of 0.1 mV s^{-1}. (b) CV curves of DCBQ at scan rates ranging from 0.1 to 0.5 mV s^{-1}. (c–f) Li^+ diffusion coefficient as a function of scan rate. (g) CV curves of W/O, PBQ, and DCBQ samples at a scan rate of 0.1 mV s^{-1}. (h, i) LSV curves derived from Figure 5g, with insets presenting the corresponding Tafel plots. (j) CV curve of a Li_2S_6 symmetric cell at a scan rate of 1 mV s^{-1}. (k) Constant potential discharge curve of a Li|Li_2S_8/tetraglyme cell at 2.05 V. (l) EIS measurements of W/O, PBQ, and DCBQ samples before cycling, with insets displaying the corresponding angular frequency plots.

organic insoluble intermediates and inorganic LiCl. This further demonstrates that the addition of DCBQ additive allows the formation of an organic–inorganic hybrid SEI layer on the electrode surface containing insoluble organic sulfur intermediates and LiCl.

CV is an important technique for verifying electrochemical reaction kinetics, as it directly reflects the reversibility and stability of the chemical reactions occurring. Additionally, CV can serve as a preliminary tool to identify the primary reaction processes and assess the diffusion rate of Li^+. Figure 5a shows the CV curves of the DCBQ additive scanned at 0.1 mV s^{-1} for different cycles. It is observed that in the first cycle, the oxidation peak potential is significantly higher than the oxidation potential after stabilization, which is due to the spontaneous discharge of polysulfides in the initial stage, where the additive does not yet play a role. Figures S9d and 5b show the CV curves of the blank electrolyte control cell and the DCBQ-added cell at different scan rates, respectively. The peak currents at different potentials are linearly fitted with respect to the scan rate, as shown in Figure 5c–f. The Li^+ diffusion

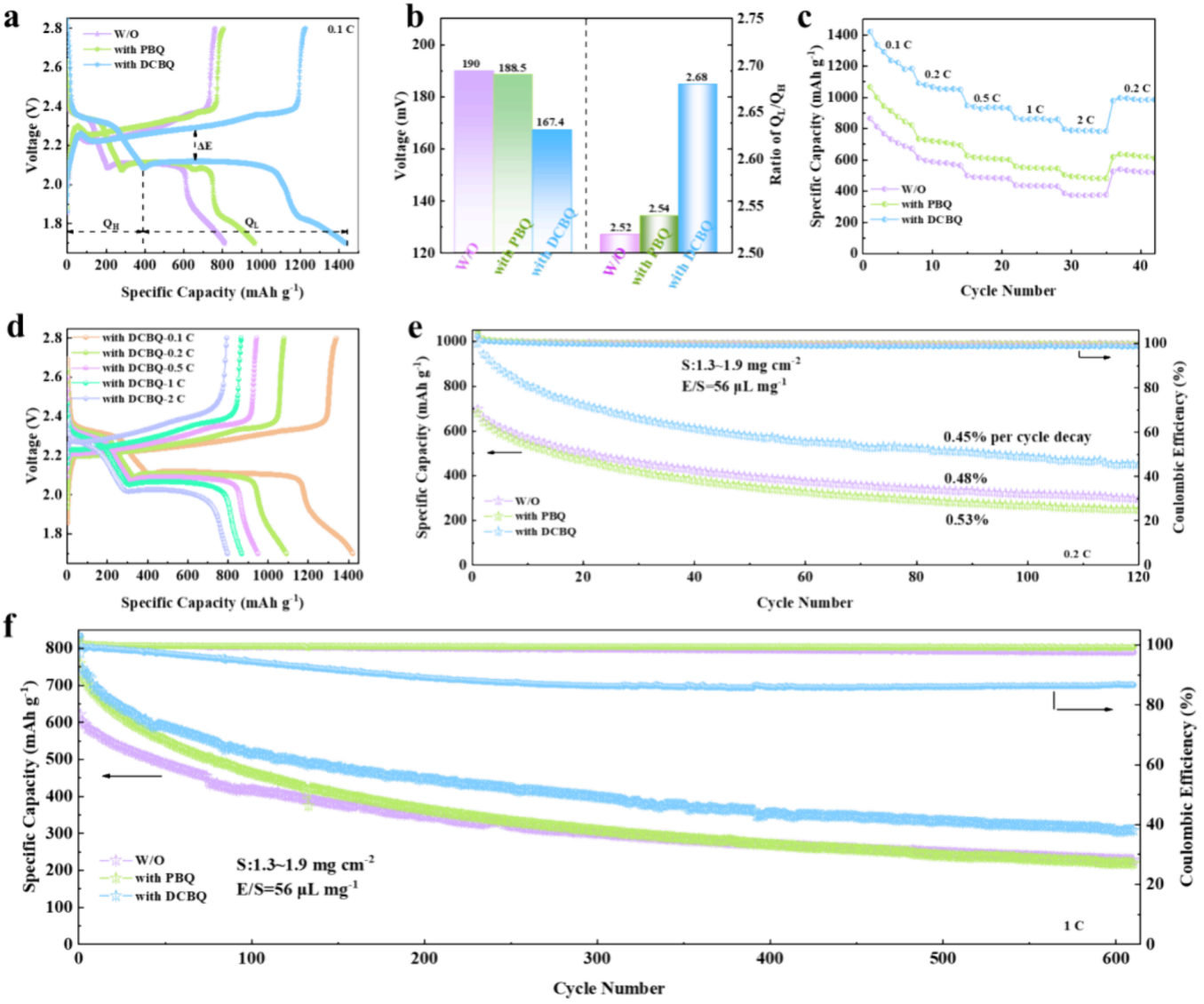

Figure 6. Performance comparison of Li−S batteries with and without three distinct quinone-based additives: (a) First-cycle charge−discharge profiles at 0.1 C for batteries with and without additives. (b) Bar graph showing the voltage difference and the ratio of low discharge platform capacity (Q_L) to high discharge platform capacity (Q_H) (Q_L/Q_H) based on the first-cycle data. (c) Rate performance curves measured at different current densities. (d) First-cycle charge/discharge profiles under varying current densities. (e) Cycling stability at 0.2 C. (f) Cycling stability at 1 C.

coefficients are calculated from different slopes based on the Randles-Sevcik equation (Supporting Information).[58] The specific values are provided in Table S2, which clearly shows that the cell containing DCBQ additive demonstrates faster reaction kinetics and higher Li^+ diffusion coefficients at every stage of the process. This suggests that DCBQ enhances the Li^+ diffusion rate throughout the entire reaction cycle. To further validate the improvement in electrochemical performance, the CV curves for the different samples (Figure 5g) reveal that all three samples display two pairs of redox peaks, confirming the reversibility of the oxidation and reduction processes of polysulfides. Among them, the DCBQ-added sample shows a narrower voltage difference (DCBQ: 240 mV, PBQ: 307 mV, W/O: 404 mV) and higher peak currents, indicating that DCBQ promotes the occurrence of redox reactions. Additionally, Figure 5h,i present Tafel slope plots and the linear sweep voltammetry (LSV) curves for the lithium deposition/dissolution process. Focusing on the process of lithium deposition, the Tafel slope values from the three samples are as follows: 106.36 (DCBQ), 141.44 (PBQ), and 139.24 mV dec^{-1} (W/O). The DCBQ sample demonstrates a lower Tafel slope, which further supports the conclusion that the inclusion of DCBQ improves the redox kinetics of polysulfides. To explore the impact of DCBQ on the redox pathway of polysulfides, CV tests on Li_2S_6 symmetric cells were performed (Figure 5j). It was observed that the addition of DCBQ resulted in an increased area of the polysulfide redox peaks and shortened the reduction pathway of Li_2S_6. Initially, the reduction process for Li_2S_6 involved the transformation from Li_2S_6 to Li_2S_4, but with DCBQ, this process was altered, facilitating the reduction of Li_2S_6 directly to Li_2S_3. This shift further accelerates the redox processes of polysulfides, highlighting that DCBQ improves the overall electrochemical activity of the polysulfide species. To confirm that DCBQ facilitates the conversion of lithium polysulfides to lithium sulfide, a constant potential lithium sulfide deposition experiment was performed. As shown in Figure 5k, DCBQ displayed a quicker response time, indicating that it enhances

the diffusion rate of Li^+ within the battery, thereby improving catalytic conversion efficiency. This is further corroborated by the impedance spectra shown in Figure 5l, which indicate that the DCBQ sample exhibited lower charge transfer resistance and enhanced ion diffusion rates. The inset slope represents the Weber factor. Based on the formula of $D = \frac{R^2T^2}{2A^2n^4F^4c^2\sigma^2}$, a smaller value of σ correlates with a stronger Li^+ diffusion coefficient.[59,60] The results in Table S3 collectively indicate that the addition of DCBQ not only promotes polysulfide conversion but also alters its primary reaction pathway. To rule out any capacity contributions from the additives during the charge−discharge process, sulfur-free batteries were assembled, and their charge−discharge profiles are depicted in Figure S10a,b. The lithium-benzoquinone batteries exhibited good redox reversibility, with stable discharge capacities and no significant degradation, indicating that the effects of PBQ and DCBQ are continuously active. However, their capacities were 0.024 mAh and 0.032 mAh, respectively, which is negligible and can be ignored in terms of the overall contribution toward the battery's capacity. To evaluate the protective effect of DCBQ on the lithium anode, Li||Li symmetric cells were fabricated to examine how the additives influence lithium deposition and dissolution processes (Figure S10c,d). The polarization voltage difference in the cells with benzoquinone additives remained stable for 300 h, with DCBQ exhibiting the lowest and most consistent polarization voltage difference (60 mV). In contrast, the cell with the blank electrolyte experienced short-circuiting, indicating that DCBQ effectively safeguards the lithium anode. To examine the stability and reversibility of the Li||Li symmetric cells, rate performance was tested in Figure S10e. The sample without additives showed a significant voltage difference at lower current densities, which suggests that polysulfides erode the lithium anode and contribute to the formation of irregular lithium dendrites. After cycling at higher current densities, the cell experienced short-circuiting, likely due to dendrites piercing the separator and creating a direct connection between the anode and cathode.[61] In contrast, the battery with DCBQ additives exhibited smaller voltage differences and less fluctuation at current densities of 0.5, 1, 2, 1, and 0.5 mA cm^{-2}, demonstrating that the addition of DCBQ greatly enhances cycling stability. This further demonstrates that the organic−inorganic hybrid SEI layer formed by the addition of DCBQ additive promotes uniform lithium deposition.

Figures 6a and 11a present the first-cycle charge/discharge curves of three prepared samples at 0.1 and 0.2 C, respectively. The sample incorporating the DCBQ additive demonstrates an initial discharge capacity of 1435 mAh g^{-1} at 0.1 C, which surpasses the PBQ sample (965 mAh g^{-1}) and the blank electrolyte sample (810 mAh g^{-1}). Moreover, the voltage distribution (ΔE) and the ratio of low discharge platform capacity to high discharge platform capacity (Q_L/Q_H) serve as critical indicators for assessing battery performance. As illustrated in Figure 6b, the battery containing DCBQ displays a lower ΔE value (167.4 mV) and a higher Q_L/Q_H ratio (2.68) in comparison to the sample without additives. In this case, the ΔE is reduced by 22.6 mV, and Q_L/Q_H ratio increases by 0.16. This indicates that DCBQ enhances the conversion of polysulfides, improving the electrochemical performance and sulfur utilization of the battery. To evaluate the reversibility and stability of the batteries, rate performance were tested at varying current densities, ranging from 0.1 to 2 C (with 1 C corresponding to 1675 mAh g^{-1}). As shown in Figure 6c, the sample with the blank electrolyte exhibited relatively low discharge specific capacity and sulfur utilization, ranging from 23.1 to 51.7% across the current densities from 0.1 to 2 C. However, the inclusion of electrolyte additives resulted in significant improvements in both discharge specific capacity and sulfur utilization. For the sample containing PBQ, sulfur utilization ranged from 30.1 to 63.7% under the same conditions. The sample with DCBQ showed the highest sulfur utilization, ranging from 47.6 to 84.9%, outperforming both the unmodified sample and the PBQ sample in terms of sulfur utilization and discharge capacity. Furthermore, after high current cycling followed by a return to 0.2 C, the DCBQ sample retained a discharge capacity of 997 mAh g^{-1} with 91.4% capacity retention, demonstrating the additive's positive impact on the battery's reversibility and stability. The comparisons of charge−discharge curves at varying current densities (Figures 6d and S9b,c) revealed that the DCBQ-containing battery maintained the characteristic charge−discharge plateau of Li−S batteries even at high rates, whereas the unmodified battery experienced considerable polarization. As the current density increased, the polarization effect became more pronounced in the unmodified sample, indicating that the DCBQ additive improves the redox kinetics of sulfur. To further assess the stability of the batteries, cycling performance was evaluated at 0.2 C (Figure 6e) and 1 C (Figure 6f), respectively. The long-cycle test at 0.2 C showed that the DCBQ-enhanced battery experienced a slower decay rate of 0.455% after 120 cycles, outperforming the other two battery samples. Additionally, to further verify that the addition of DCBQ can enhance the stability of the battery, the battery with DCBQ additive was tested under high sulfur loading and lean electrolyte conditions. As shown in Figure S11b, the capacity decay rate per cycle after 100 cycles in high-sulfur-loading and lean electrolyte conditions was 0.41%, which is 0.12% higher than the stability of the blank control group. Therefore, the addition of DCBQ additive can, to some extent, improve the stability of the battery. Collectively, these results demonstrate that the DCBQ additive not only enhances discharge specific capacity but also significantly improves cycling stability.

4. CONCLUSIONS

This study introduces 2,5-dichloro-1,4-benzoquinone (DCBQ) as an electrolyte additive that effectively alters the sulfur redox pathway, safeguards the sulfur cathode, and enhances the utilization of active materials. Gibbs free energy calculations reveal that DCBQ reacts with polysulfides to form insoluble, symmetrical cyclic organic sulfur intermediates (ΔG = −148.67 kJ mol^{-1}). This reaction serves two key functions: first, it forms a cathode-electrolyte interphase (CEI) layer on the sulfur cathode surface, which reduces the accumulation of insulating Li_2S and facilitates electron transport ($\sigma_{DCBQ\text{-}Li_2S_6}$ = 3.1×10^{-5} S mm^{-1}). Second, Raman and infrared spectroscopy analyses confirm that DCBQ stabilizes polysulfides on the cathode side, minimizing the polysulfide shuttle effect and enabling a short-chain redox pathway ($Li_2S_6 \rightarrow Li_2S_3 \rightarrow Li_2S$), thus enhancing the redox kinetics. Additionally, a small amount of polysulfides that migrate to the anode side forms an organic−inorganic SEI with DCBQ, which adheres to the lithium anode surface, preventing polysulfide-induced corrosion. This modification not only boosts Li^+ conductivity but

also improves sulfur utilization, ultimately enhancing the cycling stability of the battery. As a result, the battery with the DCBQ additive achieves an initial discharge capacity of 992.24 mAh g^{-1} at 0.2 C and exhibits a low cycle-to-cycle capacity decay rate of 0.45% after 120 cycles. By providing a novel approach to sulfur redox, this method effectively addresses several challenges faced by lithium−sulfur batteries

■ ASSOCIATED CONTENT

Supporting Information

The Supporting Information is available free of charge at https://pubs.acs.org/doi/10.1021/acsami.5c01567.

Comprehensive description of experimental procedures; characterization method; material structure analysis; characterization, electrochemical data, and comparative analysis of performance of control cells (PDF)

■ AUTHOR INFORMATION

Corresponding Authors

Jianwei Ren − *Department of Chemical Engineering, University of Pretoria, Hatfield 0028, South Africa*; Email: jianwei.ren@up.ac.za

Rongfang Wang − *College of Chemical Engineering, Qingdao University of Science and Technology, Qingdao 266042, China*; orcid.org/0000-0001-9055-7408; Email: rfwang@qust.edu.cn

Authors

Jiayi Shao − *College of Chemical Engineering, Qingdao University of Science and Technology, Qingdao 266042, China*

Hanxiao Wang − *Shandong Energy Institute, Qingdao New Energy Shandong Laboratory, Qingdao Institute of Bioenergy and Bioprocess Technology, Chinese Academy of Sciences, Qingdao 266101, China*

Xinjie Huang − *College of Chemical Engineering, Qingdao University of Science and Technology, Qingdao 266042, China*

Xianguo Ma − *School of Chemical Engineering, Guizhou Institute of Technology, Guiyang 550003, China*

Xuyun Wang − *College of Chemical Engineering, Qingdao University of Science and Technology, Qingdao 266042, China*

Hongsheng Huang − *School of Chemical Engineering, Guizhou Institute of Technology, Guiyang 550003, China*

Complete contact information is available at: https://pubs.acs.org/10.1021/acsami.5c01567

Author Contributions

J.S.: Writing−original draft, Visualization, Validation, Methodology, Investigation, Formal analysis, Data curation. H.W.: Writing−original draft, Visualization, Validation, Methodology, Investigation, Formal analysis, Data curation. X.H.: Methodology, Investigation, Formal analysis. X.M.: Writing−review and editing, Writing−original draft, Supervision, Project administration. H.H.: Writing−review &editing, Writing−original draft, Validation, Project administration, Investigation, Funding acquisition. X.W.: Visualization, Supervision, Investigation. J.R.: Writing−review and editing, Writing−original draft, Formal analysis, Conceptualization. R.W.: Writing−review and editing, Writing−original draft, Formal analysis, Project administration, Conceptualization.

Notes

The authors declare no competing financial interest.

All images/illustrations/photographs appearing in this article and SI files, including those in TOC graphics, were created by the author of this manuscript.

■ ACKNOWLEDGMENTS

The authors would like to express their gratitude for the financial support received from Natural Science Foundation of Guizhou Province (Grants No. QKHJC-ZK [2023] Key 019), Top Talent Project of Guizhou Provincial Department of Education (Grant No. QJJ [2022]084), and Key Laboratory of Energy Chemistry in Guizhou universities (Grants No. QJJ [2022]035).

■ REFERENCES

(1) Manthiram, A.; Fu, Y.; Chung, S.-H.; Zu, C.; Su, Y.-S. Rechargeable lithium-sulfur batteries. *Chem. Rev.* **2014**, *114* (23), 11751−11787.

(2) Qin, W.-C.; Qiu, B.-J.; Xue, X.-Y.; Chen, C.; Xu, Z.-F.; Zhou, Q.-Q. Droplet deposition and control effect of insecticides sprayed with an unmanned aerial vehicle against plant hoppers. *Crop Prot.* **2016**, *85*, 79−88.

(3) He, W.-S.; Liu, Q.; Yu, H.; Si, X.-J.; Zhang, J.-K. Efficient synthesis of octacosanol linoleate catalyzed by ionic liquid and its structure characterization. *J. Am. Oil Chem. Soc.* **2016**, *93*, 509−517.

(4) Shi, Z.; Sun, Z.; Cai, J.; Yang, X.; Wei, C.; Wang, M.; Ding, Y.; Sun, J. Manipulating Electrocatalytic Li2S Redox via Selective Dual-Defect Engineering for Li−S Batteries. *Adv. Mater.* **2021**, *33* (43), No. 2103050.

(5) Tahir, H. E.; Xiaobo, Z.; Zhihua, L.; Jiyong, S.; Zhai, X.; Wang, S.; Mariod, A. Rapid prediction of phenolic compounds and antioxidant activity of Sudanese honey using Raman and Fourier transform infrared (FT-IR) spectroscopy. *Food Chem.* **2017**, *226*, 202−211.

(6) Hu, X.; Shi, J.; Zhang, F.; Zou, X.; Holmes, M.; Zhang, W.; Huang, X.; Cui, X.; Xue, J. Determination of retrogradation degree in starch by mid-infrared and Raman spectroscopy during storage. *Food Anal. Methods* **2017**, *10*, 3694−3705.

(7) Yang, Y.; Zheng, G.; Cui, Y. Nanostructured sulfur cathodes†. *Chem. Soc. Rev.* **2013**, *42* (7), 3018−3032.

(8) Wu, J.; Zhang, B.; Liu, J.; Liu, S.; Yan, T.; Gao, X. Grafting and Depositing Lithium Polysulfides on Cathodes for Cycling Stability of Lithium−Sulfur Batteries. *ACS Appl. Mater. Interfaces* **2021**, *13* (34), 40685−40694.

(9) Li, M.; Lu, J.; Amine, K. Nanotechnology for Sulfur Cathodes. *ACS Nano* **2021**, *15* (5), 8087−8094.

(10) Duan, H.; Li, K.; Xie, M.; Chen, J.-M.; Zhou, H.-G.; Wu, X.; Ning, G.-H.; Cooper, A. I.; Li, D. Scalable Synthesis of Ultrathin Polyimide Covalent Organic Framework Nanosheets for High-Performance Lithium−Sulfur Batteries. *J. Am. Chem. Soc.* **2021**, *143* (46), 19446−19453.

(11) Han, X.; Zhang, Z.; Xu, X. Single atom catalysts supported on N-doped graphene toward fast kinetics in Li−S batteries: a theoretical study. *Journal of Materials Chemistry A* **2021**, *9* (20), 12225−12235.

(12) Pang, Q.; Liang, X.; Kwok, C. Y.; Nazar, L. F. Advances in lithium−sulfur batteries based on multifunctional cathodes and electrolytes. *Nature Energy* **2016**, *1*, 16132.

(13) Li, X.; Xiao, Y.; Zeng, Q.; Xu, L.; Guo, S.; Zheng, C.; Zhang, Q.; Huang, S. Manipulating Orbital Hybridization of Single-Atom Catalytic Sites in Metal-Organic Framework for High-Performance Lithium-Sulfur Batteries. *Nano Energy* **2023**, *116*, No. 108813.

(14) Zhang, X.; Yang, T.; Zhang, Y.; Wang, X.; Wang, J.; Li, Y.; Yu, A.; Wang, X.; Chen, Z. Single Zinc Atom Aggregates: Synergetic Interaction to Boost Fast Polysulfide Conversion in Lithium-Sulfur Batteries. *Adv. Mater.* **2023**, *35* (6), 2208470.

(15) Wu, J.; Ye, T.; Wang, Y.; Yang, P.; Wang, Q.; Kuang, W.; Chen, X.; Duan, G.; Yu, L.; Jin, Z.; et al. Understanding the Catalytic Kinetics of Polysulfide Redox Reactions on Transition Metal Compounds in Li−S Batteries. *ACS Nano* **2022**, *16* (10), 15734−15759.
(16) Xu, R.; Tang, H.; Zhou, Y.; Wang, F.; Wang, H.; Shao, M.; Li, C.; Wei, Z. Enhanced catalysis of radical-to-polysulfide interconversion via increased sulfur vacancies in lithium−sulfur batteries. *Chemical Science* **2022**, *13* (21), 6224−6232.
(17) Meng, T.; Geng, Z.; Ma, F.; Wang, X.; Zhang, H.; Guan, C. Direct ink writing of metal-based electrocatalysts for Li−S batteries with efficient polysulfide conversion. *Interdisciplinary Materials* **2023**, *2*, 589−608.
(18) Sun, Z.; Zhang, J.; Yin, L.; Hu, G.; Fang, R.; Cheng, H.-M.; Li, F. Conductive porous vanadium nitride/graphene composite as chemical anchor of polysulfides for lithium-sulfur batteries. *Nat. Commun.* **2017**, *8*, 14627.
(19) Xiao, Z.; Yang, Z.; Wang, L.; Nie, H.; Zhong, M. E.; Lai, Q.; Xu, X.; Zhang, L.; Huang, S. A Lightweight TiO_2/Graphene Interlayer, Applied as a Highly Effective Polysulfide Absorbent for Fast, Long-Life Lithium−Sulfur Batteries. *Adv. Mater.* **2015**, *27* (18), 2891−2898.
(20) Seh, Z. W.; Yu, J. H.; Li, W.; Hsu, P.-C.; Wang, H.; Sun, Y.; Yao, H.; Zhang, Q.; Cui, Y. Two-dimensional layered transition metal disulphides for effective encapsulation of high-capacity lithium sulphide cathodes. *Nat. Commun.* **2014**, *5*, 5017.
(21) Dong, W.; Wang, D.; Li, X.; Yao, Y.; Zhao, X.; Wang, Z.; Wang, H.-E.; Li, Y.; Chen, L.; Qian, D.; et al. Bronze TiO_2 as a cathode host for lithium-sulfur batteries. *Journal of Energy Chemistry* **2020**, *48*, 259−266.
(22) Zhang, H.; Zhao, W.; Zou, M.; Wang, Y.; Chen, Y.; Xu, L.; Wu, H.; Cao, A. 3D, Mutually Embedded MOF@Carbon Nanotube Hybrid Networks for High-Performance Lithium-Sulfur Batteries. *Adv. Energy Mater.* **2018**, *8* (19), No. 1800013.
(23) Chen, K.; Sun, Z.; Fang, R.; Shi, Y.; Cheng, H.-M.; Li, F. Metal−Organic Frameworks (MOFs)-Derived Nitrogen-Doped Porous Carbon Anchored on Graphene with Multifunctional Effects for Lithium−Sulfur Batteries. *Adv. Funct. Mater.* **2018**, *28* (38), No. 1707592.
(24) Wu, Q.; Zhou, X.; Xu, J.; Cao, F.; Li, C. Carbon-based derivatives from metal-organic frameworks as cathode hosts for Li−S batteries. *Journal of Energy Chemistry* **2019**, *38*, 94−113.
(25) Rana, M.; Luo, B.; Kaiser, M. R.; Gentle, I.; Knibbe, R. The role of functional materials to produce high areal capacity lithium sulfur battery. *Journal of Energy Chemistry* **2020**, *42*, 195−209.
(26) Jia, W.; Zheng, Y.; Zhao, D. A.; Yin, X.; Liu, X.; Du, R.; Engineering, B. Preprocessing method of night vision image application in apple harvesting robot. *Int. J. Agric. Biol. Eng.* **2018**, *11* (2), 158−163.
(27) Li, H.; Ma, S.; Li, J.; Liu, F.; Zhou, H.; Huang, Z.; Jiao, S.; Kuang, Y. Altering the Reaction Mechanism to Eliminate the Shuttle Effect in Lithium-Sulfur Batteries. *Energy Storage Materials* **2020**, *26*, 203−212.
(28) Lu, H.; Liu, M.; Zhang, X.; Chang, L.; Wang, P.; Ma, Y.; Luo, S.; Zhang, Z.; Wang, Y.; Yuan, Y. Catalytic Effect of Ammonium Thiosulfate as a Bifunctional Electrolyte Additive for Regulating Redox Kinetics in Lithium−Sulfur Batteries by Altering the Reaction Pathway. *ACS Appl. Mater. Interfaces* **2024**, *16* (11), 13640−13650.
(29) Lu, T.; Chen, Q. Independent gradient model based on Hirshfeld partition: A new method for visual study of interactions in chemical systems. *J. Comput. Chem.* **2022**, *43* (8), 539−555.
(30) Xue, C.; Wang, P.; Che, H.; Liu, W.; Liu, B.; Ao, Y. Simultaneous organic pollutant degradation and hydrogen peroxide production by molecular-engineered carbon nitride. *Applied Catalysis B: Environment and Energy* **2024**, *340*, No. 123259.
(31) Lefebvre, C.; Rubez, G.; Khartabil, H.; Boisson, J.-C.; Contreras-García, J.; Hénon, E. Accurately extracting the signature of intermolecular interactions present in the NCI plot of the reduced density gradient versus electron density. *Phys. Chem. Chem. Phys.* **2017**, *19* (27), 17928−17936.
(32) Gao, R.; Wang, K.; Wang, F.; Wang, H.; Wang, X.; Ren, J.; Wang, R. Synthetic perylenequinone as anchoring center of sulfur and catalyst for polysulfides conversion. *Chemical Engineering Journal* **2023**, *455*, No. 140847.
(33) Chen, L.; Cheng, L.; Yu, J.; Chu, J.; Wang, H. G.; Cui, F.; Zhu, G. Tailored Organic Cathode Material with Multi-Active Site and Compatible Groups for Stable Quasi-Solid-State Lithium-Organic Batteries. *Adv. Funct. Mater.* **2022**, *32* (49), No. 2209848.
(34) Zhang, H.; Zhang, R.; Ding, F.; Shi, C.; Zhao, N. Hydrogen bonding regulation enables indanthrone as a stable and high-rate cathode for lithium-ion batteries. *Energy Storage Materials* **2022**, *51*, 172−180.
(35) Barchasz, C.; Molton, F.; Duboc, C.; Leprêtre, J.-C.; Patoux, S.; Alloin, F. Lithium/sulfur cell discharge mechanism: an original approach for intermediate species identification. *Anal. Chem.* **2012**, *84* (9), 3973−3980.
(36) Lu, T.; Chen, F. Multiwfn: A multifunctional wavefunction analyzer. *J. Comput. Chem.* **2012**, *33* (5), 580−592.
(37) Wang, Z.; Liu, J.; Zhang, B.; Sun, L.; Cong, L.; Lu-Li, N.; Mauger, A.; Julien, C. M.; Xie, H.; Sun, H. Modulating molecular orbital energy level of lithium polysulfide for high-rate and long-life lithium-sulfur batteries. *Energy Storage Materials* **2020**, *24*, 373−378.
(38) Palmö, K.; Pietilä, L. O.; Mannfors, B.; Karonen, A.; Stenman, F. Raman scattering from p-benzoquinone. *J. Mol. Spectrosc.* **1983**, *100* (2), 368−376.
(39) Govindarajan, M.; Karabacak, M.; Suvitha, A.; Periandy, S. FT-IR FT-Raman, ab initio, HF and DFT studies, NBO, HOMO-LUMO and electronic structure calculations on 4-chloro-3-nitrotoluene. *Spectrochimica Acta Part a-Molecular and Biomolecular Spectroscopy* **2012**, *89*, 137−148.
(40) Nagabalasubramanian, P. B.; Periandy, S.; Mohan, S.; Govindarajan, M. FTIR and FT Raman spectra, vibrational assignments, ab initio, DFT and normal coordinate analysis of α,α dichlorotoluene. *Spectrochimica Acta Part a-Molecular and Biomolecular Spectroscopy* **2009**, *73* (2), 277−280.
(41) Suvitha, A.; Kothandan, G.; Steephen, A. Molecular structure, FT-Raman, IR, NLO, NBO, HOMO−LUMO analysis, physicochemical descriptors, adme parameters, and pharmacokinetic bioactivity of 2,3,5,6-tetrachloro-p-benzoquinone. *J. Struct. Chem.* **2021**, *62* (9), 1339−1356.
(42) Gunasekaran, S.; Thilak Kumar, R.; Ponnusamy, S. Vibrational spectra and normal coordinate analysis of diazepam, phenytoin and phenobarbitone. *Spectrochimica Acta Part A: Molecular and Biomolecular Spectroscopy* **2006**, *65* (5), 1041−1052.
(43) Pawlukojć, A.; Natkaniec, I.; Bator, G.; Grech, E.; Sobczyk, L. Inelastic neutron scattering studies on dichloro-1,4-benzoquinones. *Spectrochimica Acta Part A: Molecular and Biomolecular Spectroscopy* **2004**, *60* (12), 2875−2882.
(44) Diao, Y.; Xie, K.; Xiong, S.; Hong, X. Insights into Li-S Battery Cathode Capacity Fading Mechanisms: Irreversible Oxidation of Active Mass during Cycling. *J. Electrochem. Soc.* **2012**, *159* (11), A1816−A1821.
(45) Gu, J.; Yang, D.; Wang, X.; Song, Y.; Li, Z.; Qiu, H.; Wang, M.; Wang, Q.; Hong, B.; Zhang, Z.; et al. Ammonium benzenesulfonate as an electrolyte additive to relieve the irreversible accumulation of lithium sulfide for high-energy density lithium-sulfur battery. *J. Colloid Interface Sci.* **2023**, *629*, 368−376.
(46) Agostini, M.; Xiong, S.; Matic, A.; Hassoun, J. Polysulfide-containing Glyme-based Electrolytes for Lithium Sulfur Battery. *Chem. Mater.* **2015**, *27* (13), 4604−4611.
(47) Zhang, H.; Zuo, P.; Hua, J.; Ma, Y.; Du, C.; Cheng, X.; Gao, Y.; Yin, G. Improved Rate Performance of Lithium Sulfur Batteries by In-Situ Anchoring of Lithium Iodide in Carbon/Sulfur Cathode. *Electrochim. Acta* **2017**, *238*, 257−262.
(48) Liang, X.; Kwok, C. Y.; Lodi-Marzano, F.; Pang, Q.; Cuisinier, M.; Huang, H.; Hart, C. J.; Houtarde, D.; Kaup, K.; Sommer, H.; et al. Tuning Transition Metal Oxide−Sulfur Interactions for Long Life

Lithium Sulfur Batteries: The "Goldilocks" Principle. *Adv. Energy Mater.* **2016**, *6* (6), No. 1501636.
(49) Zhao, T.; Ye, Y.; Peng, X.; Divitini, G.; Kim, H.-K.; Lao, C.-Y.; Coxon, P. R.; Xi, K.; Liu, Y.; Ducati, C.; et al. Advanced Lithium−Sulfur Batteries Enabled by a Bio-Inspired Polysulfide Adsorptive Brush. *Adv. Funct. Mater.* **2016**, *26* (46), 8418−8426.
(50) Wang, S.; Chen, H.; Liao, J.; Sun, Q.; Zhao, F.; Luo, J.; Lin, X.; Niu, X.; Wu, M.; Li, R. Efficient trapping and catalytic conversion of polysulfides by VS4 nanosites for Li−S batteries. *ACS Energy Lett.* **2019**, *4* (3), 755−762.
(51) Xue, Y.; Luo, D.; Yang, N.; Ma, G.; Zhang, Z.; Hou, J.; Wang, J.; Ma, C.; Wang, X.; Jin, M. Engineering checkerboard-like heterostructured sulfur electrocatalyst towards high-performance lithium sulfur batteries. *Chem. Eng. J.* **2022**, *440*, No. 135990.
(52) Chen, K.; Fang, R.; Lian, Z.; Zhang, X.; Tang, P.; Li, B.; He, K.; Wang, D.-W.; Cheng, H.-M.; Sun, Z.; et al. An in-situ solidification strategy to block polysulfides in Lithium-Sulfur batteries. *Energy Storage Materials* **2021**, *37*, 224−232.
(53) Wei, J.-Y.; Zhang, X.-Q.; Hou, L.-P.; Shi, P.; Li, B.-Q.; Xiao, Y.; Yan, C.; Yuan, H.; Huang, J.-Q. Shielding Polysulfide Intermediates by an Organosulfur-Containing Solid Electrolyte Interphase on the Lithium Anode in Lithium-Sulfur Batteries. *Adv. Mater.* **2020**, *32* (37), No. 2003012.
(54) Zhang, W.; Ma, F.; Wu, Q.; Cai, Z.; Zhong, W.; Zeng, Z.; Cheng, S.; Xie, J. Bifunctional Fluorinated Anthraquinone Additive for Improving Kinetics and Interfacial Chemistry in Rechargeable Li−S Batteries. *ACS Applied Energy Materials* **2022**, *5* (12), 15719−15728.
(55) Gao, R.; Zhang, Q.; Wang, H.; Wang, F.; Ren, J.; Wang, X.; Ma, X.; Wang, R. Synergic effect of covalent and chemical sulfur fixation enhancing the immobilization-conversion of polysulfides in lithium-sulfur batteries. *Journal of Energy Chemistry* **2023**, *79*, 1−11.
(56) Gu, L.-L.; Gao, J.; Wang, C.; Qiu, S.-Y.; Wang, K.-X.; Gao, X.-T.; Sun, K.-N.; Zuo, P.-J.; Zhu, X.-D. Thin-carbon-layer-enveloped cobalt−iron oxide nanocages as a high-efficiency sulfur container for Li−S batteries. *Journal of Materials Chemistry A* **2020**, *8* (39), 20604−20611.
(57) Li, S.; Dai, H.; Li, Y.; Lai, C.; Wang, J.; Huo, F.; Wang, C. Designing Li-protective layer via SOCl2 additive for stabilizing lithium-sulfur battery. *Energy Storage Materials* **2019**, *18*, 222−228.
(58) Ding, Y.; Shi, Z.; Sun, Y.; Wu, J.; Pan, X.; Sun, J. Steering Bidirectional Sulfur Redox via Geometric/Electronic Mediator Comodulation for Li−S Batteries. *ACS Nano* **2023**, *17* (6), 6002−6010.
(59) Teo, L. P.; Buraidah, M. H.; Arof, A. K. Study on Li^+ ion diffusion in Li_2SnO_3 anode material by CV and EIS techniques. *Mol. Cryst. Liq. Cryst.* **2019**, *694* (1), 117−130.
(60) Cholant, C. M.; Azevedo, C. F.; Caldeira, I.; Balboni, R. D. C.; Moura, E. A.; Westphal, T. M.; Pawlicka, A.; Berton, M. A. C.; Gomez, J. A.; Avellaneda, C. O. Li^+ ions diffusion coefficient in V_2O_5:MoO_3 Sol-Gel films. *Mol. Cryst. Liq. Cryst.* **2017**, *655* (1), 61−70.
(61) Wood, K. N.; Kazyak, E.; Chadwick, A. F.; Chen, K.-H.; Zhang, J.-G.; Thornton, K.; Dasgupta, N. P. Dendrites and Pits: Untangling the Complex Behavior of Lithium Metal Anodes through Operando Video Microscopy. *ACS Central Science* **2016**, *2* (11), 790−801.